IEEE Access
Multidisciplinary | Rapid Review | Open Access Journal

Received 12 August 2024, accepted 8 September 2024, date of publication 16 September 2024, date of current version 26 September 2024.

Digital Object Identifier 10.1109/ACCESS.2024.3460766

RESEARCH ARTICLE

High-Efficiency Reconfigurable Single-Stage Bidirectional AC/DC Converter for 50 kW Fast Charger

MILLION GERADO GEDA[1,2], (Member, IEEE), SUNJU KIM[1], (Student Member, IEEE), AND SEWAN CHOI[1], (Fellow, IEEE)

[1]Department of Electrical and Information Engineering, Seoul National University of Science and Technology (Seoul Tech), Seoul 01811, South Korea
[2]Department of Electrical Power and Control Engineering, Adama Science and Technology University (ASTU), Adama 1888, Ethiopia

Corresponding author: Million Gerado Geda (milliongerado1023@seoultech.ac.kr)

This work was supported by the Research Program funded by Seoul National University of Science and Technology (SeoulTech).

ABSTRACT This article presents a reconfigurable single-stage AC-DC converter for fast Electric Vehicle (EV) battery charging. The proposed converter offers high power transfer capability, high efficiency, and a wide output voltage range of full Zero Voltage Switching (ZVS) turn-on, facilitated by its reconfigurable features and an additional control variable. Low rating relays are installed on the secondary side of transformers to diversify output battery voltages. These relays are pre-set before the charging process begins, based on EV battery class, as changing relays during the charging process could lead to dynamic issues due to its low-speed operation. In addition, control variables of the proposed converter are optimized to reduce switching losses, conduction losses, and grid current total harmonic distortion (THD). Therefore, the proposed converter provides efficient and reliable charging for both 400 V and 800 V class EV batteries. An 8.4 kW fast charger laboratory prototype module is built and tested to validate theoretical claims at grid input voltage of 230 V, and battery voltages from 150 V to 920 V. As a result, peak efficiency of 97.15% is achieved. Above all flat efficiency power conversion is achieved according to charging line.

INDEX TERMS Fast charger, high efficiency, reconfigurable single-stage AC-DC converter, wide output voltage range.

I. INTRODUCTION

Charging infrastructure for Electric Vehicle (EV) with high efficiency, fast charging time, bi-directional capability, and high-power quality is crucial [1], [3], [4], [5]. The development of suitable converters, along with optimized design and control strategies, is essential to meet these requirements.

Nowadays two-stage converters are widely used for fast chargers [6], [7], [8], [9]. The Vienna rectifier is among the widely used two-stage EV charger converters [9], [10].

In addition, commercial fast chargers such as the ABB Terra 184 CC HVC fast charger [7], [8], Tesla super-charger V_2, Porsche Modular Fast Charging Park A, and ENERCON E-Charger 600 model are built using two-stage converters [11]. These converters use electrolytic DC link capacitors; however, electrolytic capacitors have a shorter lifespan (lower reliability) and higher maintenance costs compared to film and MLLC capacitors. Furthermore, two-stage converters have lower efficiency due to their two conversion stages, and most of commercial two-stage fast chargers are unidirectional [7], [8], [11].

However, single-stage converters offer higher power density, higher reliability, and longer lifespan by eliminating electrolytic capacitors compared to two-stage converters [12], [13], [14], [15]. This allows for the use of film or MLCC capacitor instead of bulky electrolytic DC link capacitors. Additionally, they can achieve higher efficiency due to their single-stage conversion [12], [13].

The high efficiency of conventional single-stage converters is limited to a narrow output battery voltage (V_B) range due to their restricted voltage gain. It becomes severe for

The associate editor coordinating the review of this manuscript and approving it for publication was Kai Song.

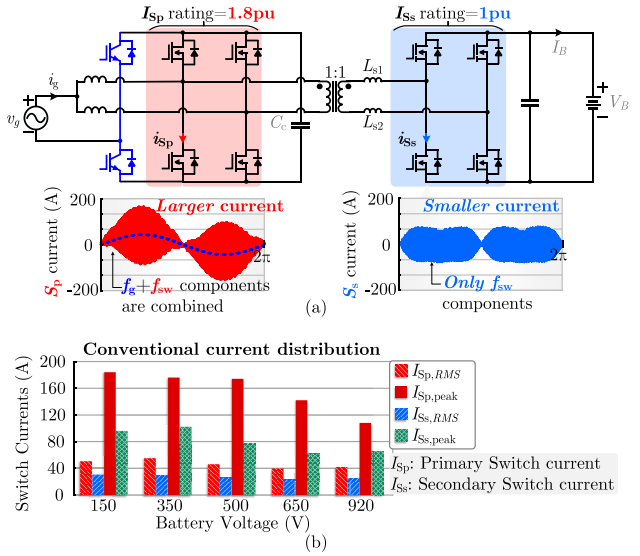

FIGURE 1. Primary and secondary switch current composition of conventional topology [12]. (b). Magnitude of primary and secondary switch current according to charging line given in Fig. 9(a).

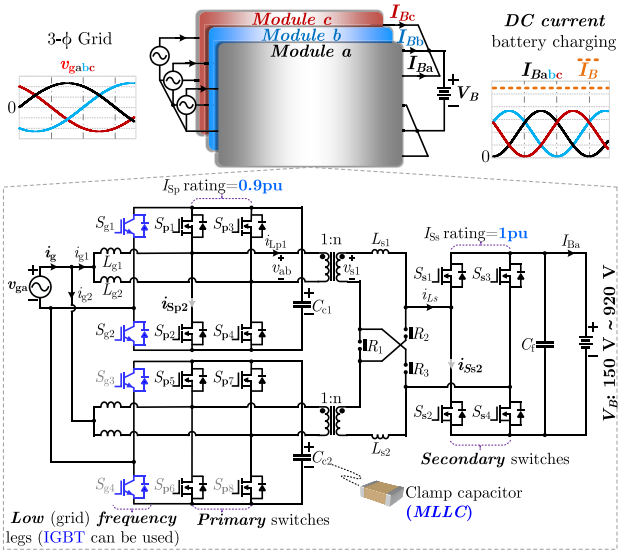

FIGURE 2. Proposed single-stage fast-charger converter with DC current output for 3-ϕ input without need of large DC link capacitor.

two-stage converters that already achieved low efficiency due to their two stages conversion. Reduced conversion efficiency over a wide output voltage range is mainly caused by severe hard-switching and high circulation power [14], and it becomes worse as operation points far from optimal voltage gain conditions [16].

Various modulation strategies and controls have been introduced for single-stage converters to achieve a wide output V_B range [13], [14], [16]. However, it is yet difficult to satisfy the ultra-wide output V_B range demand by fast chargers efficiently. A fast charger should satisfy both 400V and 800 V battery class EVs simultaneously.

However, single-stage converters introduced in [12], [13], [16], and [17] are only suitable for either 400 V or 800 V class battery chargers, depending on their designed transformer turn ratio. Using these converters for both battery class can lead to a significant reduction in efficiency and severe Electromagnetic Interference (EMI) due to hard switching (HS) turn-on and large circulating currents, depending on the converter design and V_B range [14], [18].

The output V_B range of a fast charger typically spans from 150 V to 920 V [19], [20], [21]. Various DC relay configurations have been adopted to accommodate such a wide V_B ranges [7], [8], [11], [21]. However, high-voltage and high-current rated relays are needed as they are installed at the battery terminals. Additionally, DC relays are more expensive compared to AC relays with equivalent ratings.

Furthermore, the primary side of conventional single-stage converter is composed of Power Factor Correction (PFC) and the primary DC-DC part of two-stage converter [12], [13], [16]. This means it integrates grid frequency (f_g) current from PFC and switching frequency (f_{sw}) current from primary DC-DC part of two-stage converter. As a result, the primary switch of a single-stage converter must handle a larger current, nearly twice that of the secondary switches, as shown in Fig.1(a) and 1(b). This situation is worse with single-stage converters with primary half-bridge type [16], [17]. Single-stage converters introduced in [22] and [23] may achieve similar primary and secondary current ratings, but they have narrow voltage range.

A switch with a larger current rating could be used on the primary side. However, it is challenging to obtain high-current rating Silicon Carbide (SiC) MOSFETs to meet the growing demand for high-power fast charging, such as 50kW per module and beyond. Therefore, double primary bridges with lower current rating switches could be used.

This article introduces a high-power, reconfigurable single-stage converter adaptable for both 400 V and 800 V class EV battery charging, as shown in Fig.2. This converter allows for the use of switches with the same rating on both the primary and secondary sides. Proposed structure was introduced in [24], but it lacks optimization, analysis and experimental results.

The proposed converter features an AC relay structure installed on the secondary side to accommodate different output V_B levels for both battery classes. Unlike previous designs that use DC relays, this design employs lower voltage and current rating AC relays, which are more cost-effective. Importantly, the relays remain unchanged during the charging process; instead, they are pre-set according to the battery class before charging begins, that enhances the reliability of the fast charger.

Proposed relay structure can be applied to various single-stage converters [13]. However, switch current utilization factor should be considered while selecting primary bridges. Features of the proposed converter includes:

1) High power transfer capability with easy scalability.
2) Using the same switches on both sides to reduce costs by lowering the unit price in mass production.

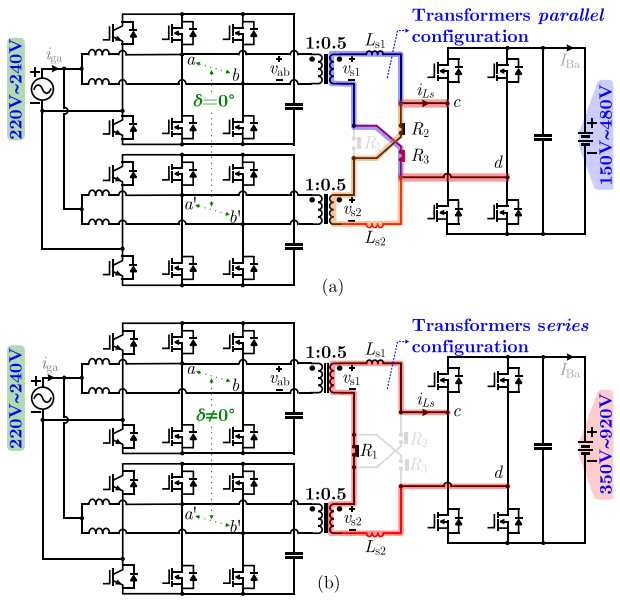

FIGURE 3. Relays configuration (setup) for both battery class EVs (a) 400 V class EV. (b) 800 V class EV.

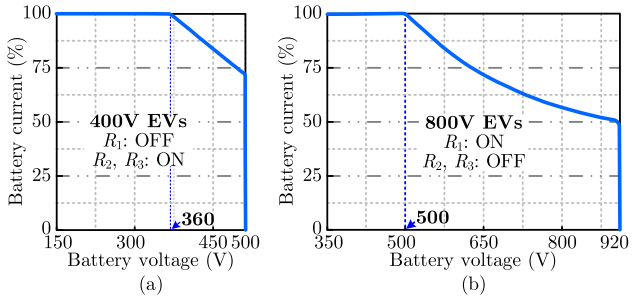

FIGURE 4. Exemplary operating charging lines of proposed converter configurations [25], [26]. (a) For 400 V class EV. (b) For 800 V class EV.

3) Wide ZVS turn-on from 150 V to 920 V.
4) Reduced circulating current and low conduction loss.
5) Flat-efficiency conversion entire the charging line.
6) Improved power quality with the proposed control strategy.

II. PROPOSED TOPOLOGY AND ITS OPERATING PRINCIPLE

A. TOPOLOGY

Fig. 2 shows the proposed single-stage converter designed for fast charger applications. The primary bridges are paralleled to reduce current stress on primary switches. As a result, the primary switches of the proposed converter achieve a similar current rating (0.9 pu) as the secondary switches (1 pu).

The overall size of the input inductor (L_g) and clamp capacitor (C_c) in the proposed converter is comparable to that of the conventional converter shown in Fig.1, at the same power level. However, in the proposed converter, these large components are divided into smaller units. Additionally, relay costs can be quickly recouped due to the high efficiency of the proposed converter. Therefore, the proposed converter is cost-effective, and easy to increase power to satisfy the growing demand of today's high power charging requirement such as 50 kW, 100 kW and higher for 3-phase grid input while using same rating switches for primary and secondary side. Relay structures on secondary side of the transformer provide the following advantages:

1) They diversify the equivalent output voltages of transformers (v_s) under 400 V and 800 V class batteries, as shown in Fig. 6(a) and 6(b), respectively. This increases the efficiency of the converter by achieving ZVS turn-on and reducing circulating power.
2) They diversify the equivalent series inductance (L_s) ensuring optimal power transfer of the charger in both parallel and series configurations, as illustrated in Fig. 6. This capability is not achievable with conventional relay structures [7], [8], [11], [21].

IGBTs could potentially replace relays; however, relays are preferred due to their lower conduction losses and cost. Grid frequency switches (S_g) synchronized with grid polarity, while primary switches (S_p) and secondary switches (S_s) operate at f_{sw}. The second-order DC currents output by each module are interleaved by 120° to produce a pure DC battery current (I_B) under a 3-phase input, as shown in Fig. 2. This allows for the use of smaller clamp capacitors (film or MLCC) instead of bulky electrolytic capacitors typically used in two-stage converters.

B. OPERATION PRINCIPLE OF THE PROPOSED TOPOLOGY

The proposed converter relies on pre-relays configuration according to EV battery class, as shown in Fig. 3(a) and 3(b). Importantly, the relays do not change during the charging process. Instead, they are set in advance before the charging begins. These configurations serve to diversify the magnitudes of v_s and L_s, enabling a wide output V_B range and optimal output power under both configurations, respectively. The equivalent values of all parameters for each configuration are provided in TABLE 1.

1) PARALLEL CONFIGURATION (400V CLASS EV)

Fig. 3(a) shows 400 V EV battery class charging setup, where R_1 is OFF, while R_2 and R_3 remain ON. The output voltages of each transformer (v_{s1} and v_{s2}) are configured in parallel through L_{s1} and L_{s2} to supply the corresponding low v_{cd}. This structure utilizes stepped-down v_{s1} and v_{s2} in a parallel configuration ($v_s = v_{s1} = v_{s2}$) to efficiently handle 400 V class charging lines, shown in Fig. 4(a). With this configuration, the efficiency of the proposed converter significantly increased at low V_B due to reduced conduction and switching losses.

The value of L_s reduces due to parallel configuration of L_{s1} and L_{s2}, as illustrated in Fig. 6(a). This adjustment helps to compensate for the power transfer capability of this setup that would have been reduced due to reduced v_s and low V_B operation. The power transfer capacity of this configuration remains high due to the inverse relationship between output power and L_s, as given in (2).

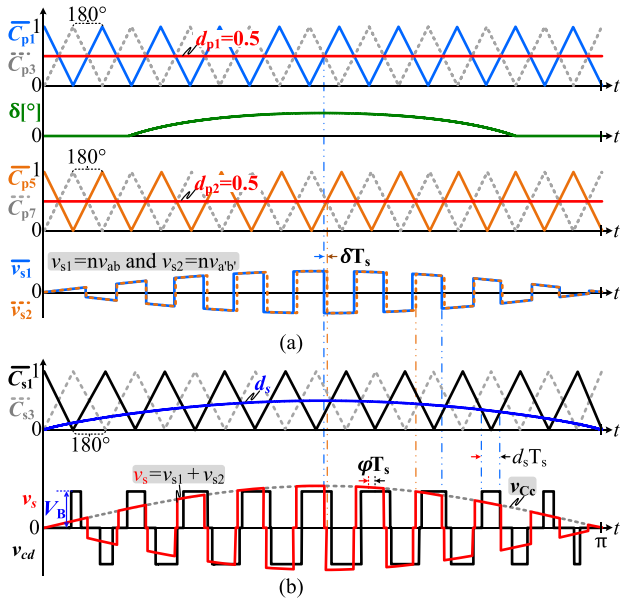

FIGURE 5. Modulation scheme. (a) Primary carrier signals, primary duty, and v_s construction. (b). Secondary carriers, secondary duty, and v_{cd} construction.

2) SERIES CONFIGURATION (800V CLASS EV)

Fig. 3(b) shows 800V class EV battery charging setup, where R_1 is ON, while R_2 and R_3 are OFF. Secondary terminals of transformers are configured in series ($v_s = v_{s1} + v_{s2}$) to efficiently deal with 800 V class charging lines, shown in Fig. 4(b). Besides, the proposed relay structure satisfied larger L_s design requirement due to series combination of L_{s1} and L_{s2}, as illustrated in Fig. 6(b). Therefore, this configuration can achieve similar output power capability as parallel configuration.

Due to its parallel or series reconfigurable capability, the proposed converter can efficiently accommodate various charging lines such as [19], [20], and [21] efficiently.

III. PROPOSED MODULATION STRATEGY AND POWER ANALYSIS OF PROPOSED CONVERTER

A. PROPOSED MODULATION SCHEMES

Fig. 5 illustrates key waveforms of the proposed modulation scheme. The primary duty cycles (d_{p1} and d_{p2}) are fixed at 0.5 to achieve ripple-free grid current (i_g). The primary carrier signals (C_{p1}, and C_{p3}) are out of phase by 180° to fully interleave input inductor currents, i_{Lg1} with i_{Lg2} and i_{Lg3} with i_{Lg4}. Transformers input voltages (v_{ab} and $v_{a'b'}$) are constructed by multiplying the switching functions of primary bridges with the corresponding voltage across clamp capacitors (v_{Cc1} and v_{Cc2}).

In series the configuration, phase shift between v_{s1} and v_{s2} (δ) can be introduced, as illustrated in Fig. 5. The magnitude of δ can be determined as given in (1). The advantage of using δ is to regulate the pulse width of v_s according to grid input and battery output voltages. This approach helps to extend ZVS turn-on voltage by introducing Triple Phase Shift (TPS), while also achieving ripple-free i_g. In addition, it optimizes conduction loss by reducing transformer series inductor current (i_{Ls}). Conventional single-stage topology [12] cannot achieve ripple-free i_g while implementing TPS. Furthermore, δ can be set to zero in a parallel configuration, as it does not significantly improve conduction or switching losses.

Secondary carrier signals (C_{s1} and C_{s3}) are out of phase by 180°. Secondary duty cycle (d_s) is generated from a simple Lookup table according to input and output voltage to achieve full ZVS turn-on [27]. The phase shift between v_s and v_{cd} (φ) is generated from AC grid input current controller, and it helps to control magnitude and direction of power, as discussed in Chapter IV.

TABLE 1. Description and equivalent values of parameters under series and parallel configurations ($L_{s1} = L_{s2}$).

Symbol	Description	Parallel config.	Series config.
d_p	Pulse-with of v_s	$d_{p1} = d_{p2} = 0.5$	$0.5\text{-}\delta = 0.5\text{-}\delta$
v_{Cc1}, v_{Cc2}	Clamp capacitor voltages	$\lvert v_g\rvert/(1\text{-}d_{p1})$	$\lvert v_g\rvert/(1\text{-}d_{p1})$
v_{Cc}	Envelope of v_s	$nv_{Cc1} = nv_{Cc2}$	$n(v_{Cc1} + v_{Cc2})$
V_{Cc}	The peak value of v_{Cc}	$nV_{Cc1} = nV_{Cc2}$	$n(V_{Cc1}+V_{Cc2})$
L_s	Total DAB inductance	$0.5L_{s1} = 0.5L_{s2}$	$2L_{s1}=2L_{s2}$
$V_{B\text{-}Nom}$	Nominal battery voltage	330V	660V

B. EQUIVALENT CIRCUIT AND POWER ANALYSIS

Fig. 6(a) and 6(b) show equivalent circuits of parallel and series configurations, respectively. These representations simplify power analysis and system design. The goal of power analysis is to optimize control variables and passive components design. The equivalent values of some parameters are diversified under each configuration, as given in TABLE 1. For example, the magnitude of v_s is reduced in parallel configuration due to parallel connection of v_{s1} and v_{s2} to accommodate 400 V V_B and, vice versa.

Most of single-stage DAB converters consist of four control variables: d_p, d_s, f_{sw}, and φ. Each control variable can be optimized to achieve specific optimization objectives. For instance, d_{p1} and d_{p2} are fixed at 0.5 to achieve a ripple-free grid current [12], and d_s can be adjusted according to input and output voltage to achieve ZVS turn-on [27]. Power is controlled by φ, and it ensures high power quality control. Meanwhile, δ is used to adjust the width of v_s to optimize conduction loss and switching loss while d_{p1} and d_{p2} remain fixed at 0.5.

The power equation for the proposed converter, involving these control variables, can be determined as given in (2), considering both inner and outer mode DAB operations, as discussed in [27]. The values of v_{Cc} and L_s, and d_p are diversified, as given in TABLE 1. Therefore, the proposed converter can output higher power even at low V_B. This capability can be proved by using these parameters in (2).

$$\delta = 360\frac{(0.5v_{Cc} - d_s V_B)}{v_{Cc}},\ if\ \delta > 0° \text{ and } \delta < \varphi, \text{ else } \delta = 0° \tag{1}$$

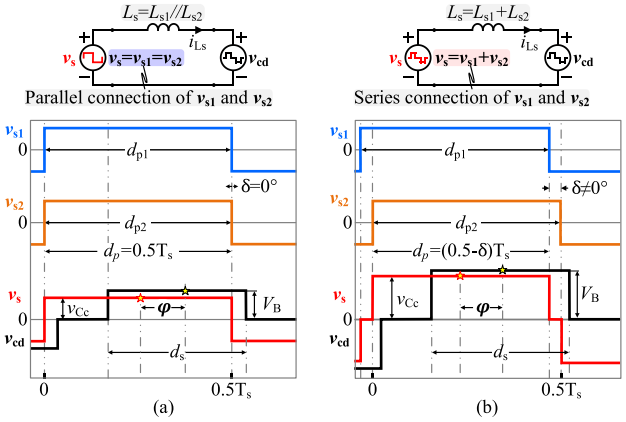

FIGURE 6. Equivalent circuits, parameters, DAB input and output voltage construction. (a) Parallel configuration. (b) series configuration.

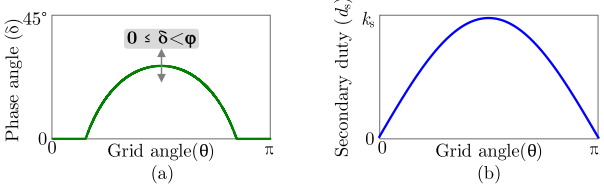

FIGURE 7. Control variables. (a) Phase shift between primary bridges (δ). (b). Secondary duty cycle (d_s), where k_s is the peak value of d_s.

$$p_o = \begin{cases} \dfrac{2v_{Cc}V_B d_s \varphi}{L_s f_{sw}}, \text{ in inner mode. Where,} \varphi \text{ is in radian.} \\ \dfrac{-V_B v_{Cc}\left[8\varphi^2 - 4\varphi - 2d_p^2 + 2d_p - 2d_s^2 + 2d_s + 1\right]}{4L_s f_{sw}}, \\ \text{in outer mode} \end{cases} \tag{2}$$

C. ZVS TURN-ON ANALYSIS

The proposed converter achieves wide ZVS turn-on with a little optimization effort due to its reconfigurable features as discussed above. The ZVS turn-on of single-stage converters depends on voltage conversion ratio (the ratio of output voltage to input voltage) termed as voltage gain [16]. However, this alone may not evaluate ZVS turn-on of the converter. In this article, voltage gain is generally described by considering not only the magnitude of the DAB output-to-input voltage ratio but also the adjustment of its pulse width (duty cycles); hence, it is referred to as volt-sec voltage conversion gain (M_{vs}). The magnitude of M_{vs} can be determined as given in (3), where v_{Cc} is the envelope of v_s, V_B is the peak value of v_{cd}, and d_p is the pulse width of v_s, as illustrated in Fig. 8. The term volt-second demonstrates the multiplication of duty and voltage.

$$M_{vs} = \frac{V_B}{v_{Cc}} \cdot \frac{d_s T_s}{d_p T_s} = \frac{V_B}{v_{Cc}} \cdot \frac{d_s}{d_p}, \text{Where } d_p = 0.5 - \delta \tag{3}$$

The value of M_{vs} is adjusted to near unity as soon as possible by adjusting d_s and/or δ, as illustrated in Fig. 8. This adjustment reduces circulating current and improves ZVS turn-on range, as the pulse width of v_s and v_{cd} can be adjusted according to input and output voltages. Specifically,

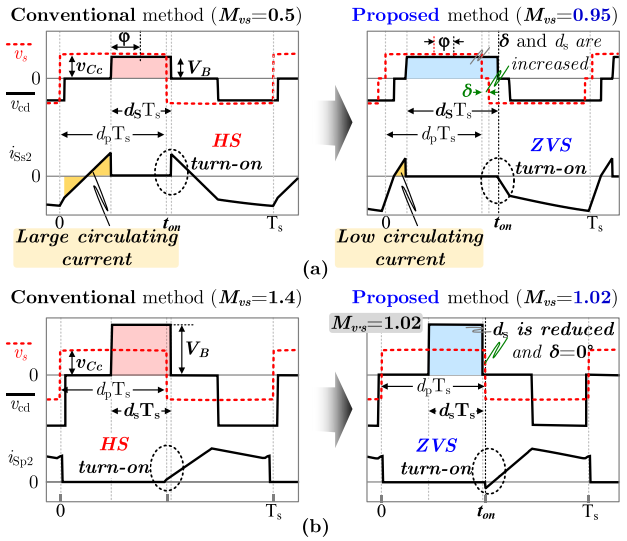

FIGURE 8. Circulating current and ZVS evaluation of conventional [12] and proposed method applied to Fig. 3(b), where [V_g = 230 V, θ = 0°]. (a) V_B = 360 V. (b) V_B = 850 V.

the magnitude of d_s increases at low V_B and decreases at high V_B, as shown in Fig. 8(a) and 8(b), respectively. Similarly, δ is increased when v_s is much larger than v_{cd}, and decreased or set to zero when v_s is much smaller than v_{cd}. This optimization technique enhances the conversion efficiency over a wide range of V_B, though it may not fully meet the ultra-wide V_B range of fast chargers.

In addition, ZVS turn-on of the proposed converter depends on the designed values of transformer turn-ratio (n) and L_s, and f_{sw}. These parameters are optimally designed based on efficiency constraints. The minimum ZVS current ($i_{ZVS-min}$) required to fully discharge C_{oss} is determined based on conservation of energy as given in (4), where V is the voltage across the equivalent drain-source capacitance and L is the inductance involved in commutation. The primary and secondary ZVS turn-on currents of the converter are given in (5) and (6), respectively based on Fig. 8.

$$i_{ZVS\,\min} \geq = \sqrt{\frac{2C_{oss}}{L_s}} \tag{4}$$

$$i_{Sp2-ZVS}(t_{on}) = i_{Lg1}(t_s) - \frac{2\varphi V_B - d_s V_B + d_p v_{Cc}}{2L_s f_{sw}} < i_{ZVS-\min} < 0 \tag{5}$$

$$i_{Ss2-ZVS}(t_{on}) = \frac{d_s V_B + 2\varphi v_{Cc} - d_s v_{Cc}}{2L_s f_{sw}} < i_{ZVS-\min} < 0 \tag{6}$$

Fig. 9(a) shows ZVS turn-on ranges of conventional single-stage converters [12], [13]. Fig. 9(b) and 9(c) show ZVS turn-on ranges of proposed converter under 400 V and 800 V class EV, respectively. This comparison is made under optimal conditions for both topologies. However, conventional converter [12], [13] achieved HS turn-on throughout the entire low V_B range. This resulted in reduced conversion efficiency under 400 V class battery charging.

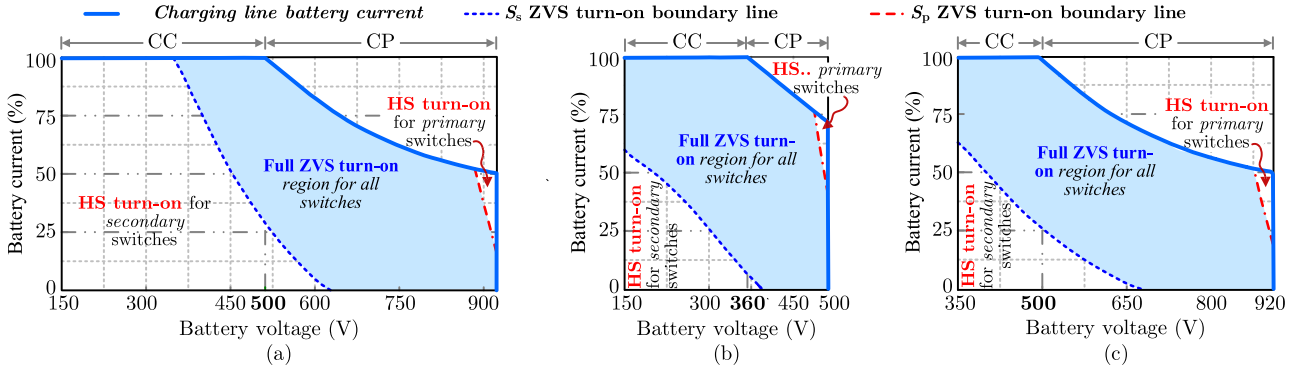

FIGURE 9. The ZVS turn-on ranges according to charging Line. (a) Conventional converter shown in Fig.1. (b) Proposed converter under 400 V class battery. (c). Proposed converter under 800 V class battery. (Note: battery current in constant current (CC) mode is considered as 100%).

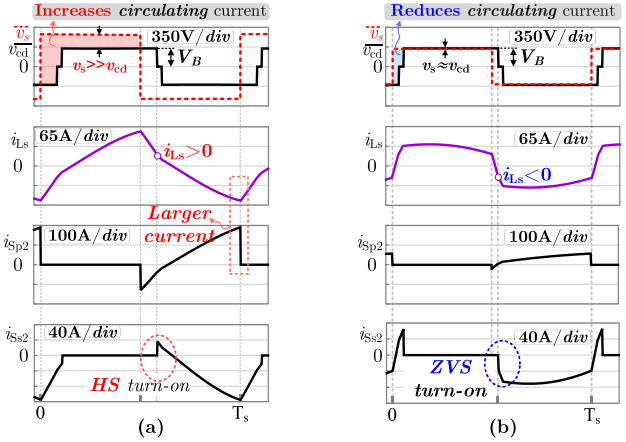

FIGURE 10. Performance evaluation according to charging line shown in Fig. 9(a) at $V_B = 300$ V, $V_g = 230$ V, and $\theta = 80°$. (a) Conventional topology [12]. (b). Proposed topology.

However, the proposed converter achieved ZVS turn-on under both 400 V and 800 V class EVs due to its reconfigurable future, with a little optimization effort mentioned above. As a result, flat conversion efficiency is achieved according to charging line. Hard-switching turn-on can be ignored at light load operation because fast chargers usually operate at full load [28].

Fig. 10(a) and 10(b) show the performance of the conventional and proposed converters at a low V_B of 300 V. The conventional converter achieved HS turn-on and large circulating current, whereas the proposed converter achieved ZVS turn-on and low circulating current due to the reduced potential between v_s and v_{cd}.

D. PARAMETERS DESIGN CONSIDERATIONS

1) CLAMP CAPACITORS

Clamp capacitor (C_{c1}) can be designed based on the clamp capacitor voltage ripple (Δv_{Cc1}) and its RMS current (I_{Cc1}) constraint over a half-switching period, as given in (7).

$$C_{c1} = C_{c2} = \frac{I_{Cc1} \cdot \mathrm{T_s}/2}{\Delta V_{Cc1}} \approx 1.6\mu\mathrm{F} \tag{7}$$

TABLE 2. Transformers design parameters.

Parameters	Values
Primary winding	0.12/300
Secondary winding	0.12/600
Magnetizing inductance (L_m)	1 mH
Leakage inductance (L_k)	1.8 µH
Turn ratio (N_p:N_s)	20:10
Core type	PQ50/50

2) TRANSFORMERS TURN RATIO

Transformer turn ratio (n) is designed equally for both transformers at nominal points to achieve similar performance among primary bridges, as given in (8) where $V_{\mathrm{B-nom}}$ is nominal V_B, and V_{Cc} is the peak value of v_s. The values V_{Cc} and $V_{\mathrm{B-Nom}}$ are provided in TABLE 1. Series configuration is considered for design.

$$n = \frac{0.5V_{B-Nom}}{V_{Cc}} = \frac{0.5 \cdot 680}{660} \approx 0.5 \tag{8}$$

3) TRANSFORMER DESIGN SPECIFICATIONS

Both transformers are designed identically for equal power distribution among primary bridges. The detail transformer design and parameters are given in TABLE 2.

4) SERIES INDUCTORS

Transformer series inductors (L_{s1} and L_{s2}) can be designed based on efficiency constraints. Peak efficiency depends on load level. Load level is determined by φ, which can be calculated as given in (9). The peak value of φ (φ_{peak}) found in the outer mode operation at grid angle of 90° [27]. It can be simplified as given in (10) where d_p and d_s are set to 0.5. In this work, peak efficiency is achieved at a nominal point when the peak value of φ (φ_{peak}) is set at 1.04 radian. Finally solving for L_s and using $V_{\mathrm{B-Nom}} =$ 660 V, $V_{Cc} = 680$ V, $f_{sw} = 130$ kHz and instantaneous peak

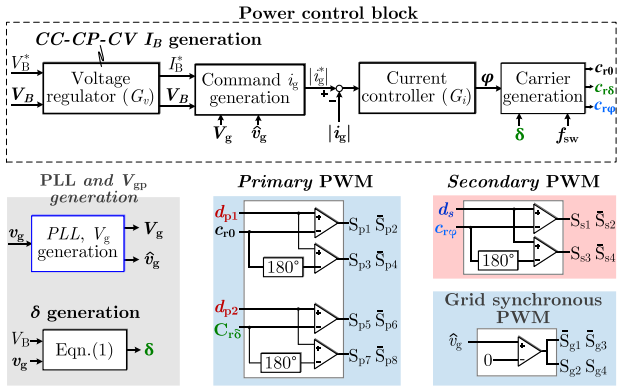

FIGURE 11. Proposed control block diagram for the proposed converter.

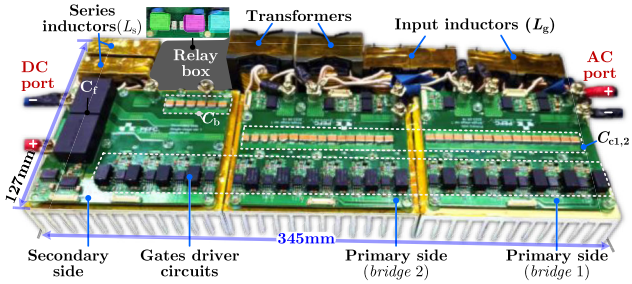

FIGURE 12. An 8.4kW laboratory prototype of proposed fast charger module.

power $(V_g \cdot I_g) = 16.8$ kW in (11), L_{s1} and L_{s2} are designed to be 10μH.

$$\varphi = \begin{cases} 2\pi \frac{L_s f_{sw} v_g i_g}{L_s f_{sw}}, \text{ (in inner mode)} \\ \frac{\pi}{2} - \pi\sqrt{-\frac{1}{4} - d_p^2 + d_p - d_s^2 + d_s - \frac{2L_s f_{sw} v_g i_g}{V_B v_{Cc}}} \\ \text{(in outer mode)} \end{cases} \tag{9}$$

$$\varphi_{\text{peak}} = \varphi(\theta = 90°) \leq \frac{\pi}{2} - \pi\sqrt{\frac{1}{4} - \frac{2L_s f_{sw}(V_g I_g)}{V_B V_{Cc}}} \approx 1\ rad. \tag{10}$$

$$L_{s1} = L_{s2} = 0.5L_s \leq 0.02768\frac{V_B V_{Cc}}{V_g I_g f_{sw}} \approx 10\mu H \tag{11}$$

5) OUTPUT FILTER CAPACITOR

Output filter capacitor (C_f) can be determined based on allowable V_B ripple (ΔV_B) constraint to suppress high frequency (f_{sw}) components from the output battery current of each module ($I_{\text{Ba,b,c}}$), as given in (12).

$$C_{\text{f}} = \frac{I_{\text{Ba}} \cdot \text{T}_{\text{s}}/2}{\Delta V_{\text{B}}} \approx 10\mu\text{F} \tag{12}$$

IV. PROPOSED CONTROL METHOD

The conventional control method achieved low power quality while implementing DC control of grid current after d-q transformation [12], [29] because the non-linear relationship between the power and its control variables was ignored. Modulation scheme involving four control variables;

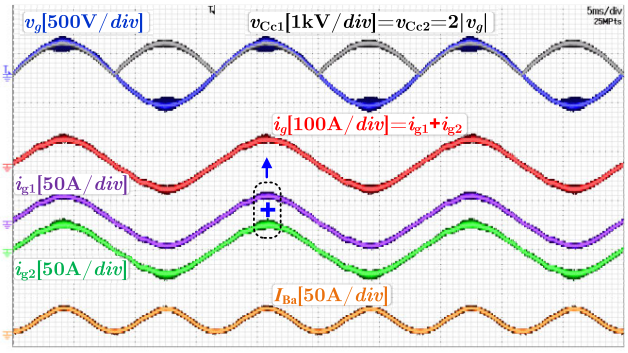

FIGURE 13. Power distribution (equal) among primary bridges.

TABLE 3. Parameters and specifications of the proposed converter (V_g = 230V, V_B = 150V to 920 V, f_{sw} = 130 kHz, P_o = 8.4 kW).

Parameters and symbols	Designed values/Types
Input inductors (L_g)	35µH, SAMHWA ELECTRIC
Series inductors (L_{s1}, L_{s2})	10µH, SAMHWA ELECTRIC
Switches (S_p, S_s)	AIMCQ120R030M1T
Clamping capacitors (C_{c1}, C_{c2})	16×GCJ55DR73A104KXJ1L
Output Capacitor (C_f)	2×MKP1848S62010JY5F
Relays (R_1, R_2, R_3)	3×HE1AN-P-DC12V-Y5

φ, d_p, d_s, f_{sw} based on a Lookup table and calculation was introduced in [13]. However, [13] is complicated to implement due to heavy calculations that require a large memory size.

Fig.11 shows the proposed control structure based on single-control variable, φ. The outer loop generates the command input grid peak current (I_g^*) according to the charging line. Command grid input peak current (I_g^*) is multiplied with the normalized grid voltage ($\hat{v}_g$) for unity Power Factor (PF), to generate AC input command current (i_g^*). However, i_g^* should be delayed by PF in case of non-unity PF that is not discussed here. An inner loop current controller generates φ, that is responsible for power control. The inner loop controls rectified AC input current (i_g) without losing its instantaneous information to achieve high input power quality by using proportional integral controller. The polarity of power can be controlled by multiplying the φ, output by controller with the required polarity (sign) of power.

V. EXPERIMENT RESULTS

An 8.4 kW single module laboratory prototype of the proposed fast charger is constructed and tested to confirm the validity of the proposed concept, as shown in Fig.12. With this prototype 25 kW output power can be achieved by implementing a 3-phase structure shown in Fig. 2.

Therefore, this prototype is designed at 50% scaled down of proposed 3-phase 50 kW fast charger. The system and design parameters of the designed prototype are given in

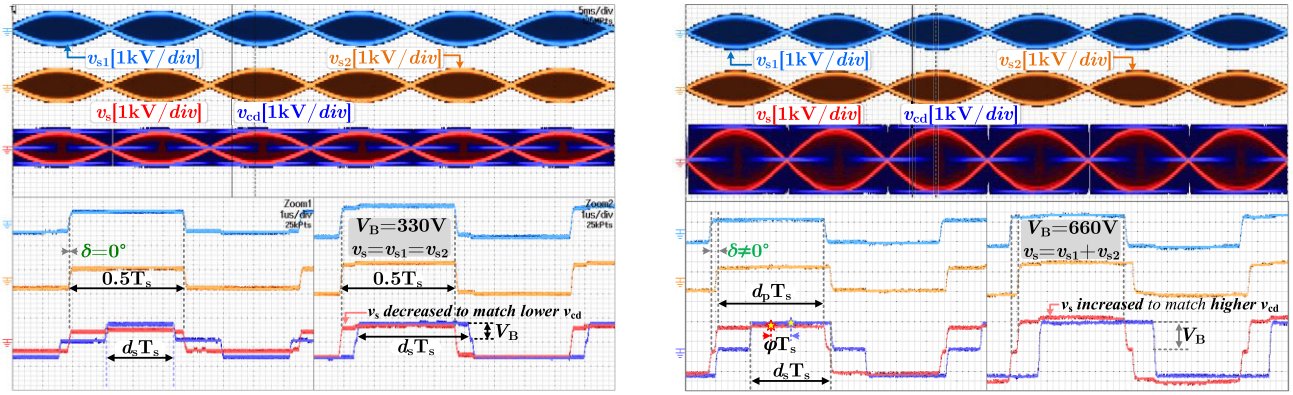

FIGURE 14. Waveforms showing how to construct v_s (where V_g = 230 V): (a). Parallel configuration at V_B = 330 V. (b) Series configuration at V_B = 660 V.

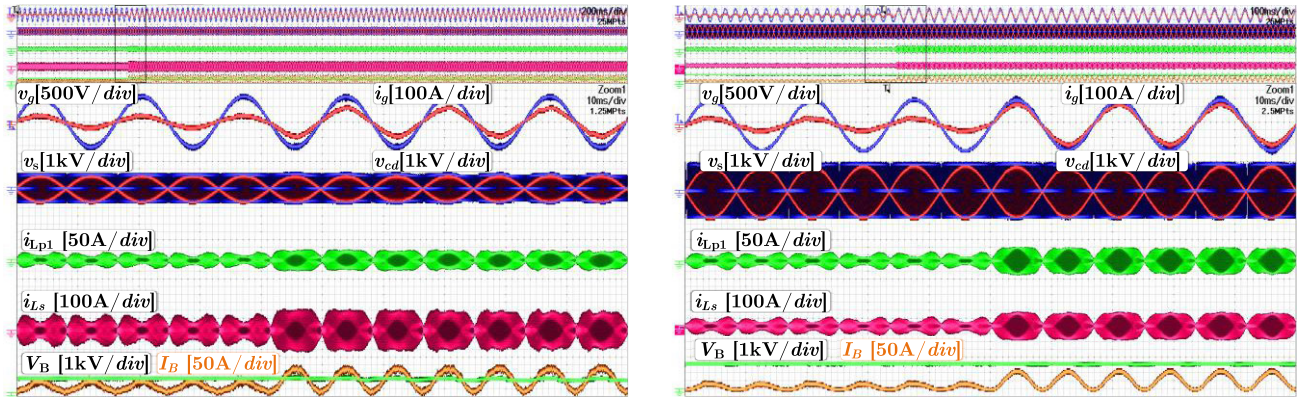

FIGURE 15. PFC and key waveforms of the proposed configurations with dynamic load change. (a). Parallel configuration for 400V class EV (P_o = 5.5 kW, V_g = 230 V, V_B = 330 V). (b). Series configuration for 800 V class EV (P_o = 8.4 kW, V_g = 230 V, V_B = 660 V).

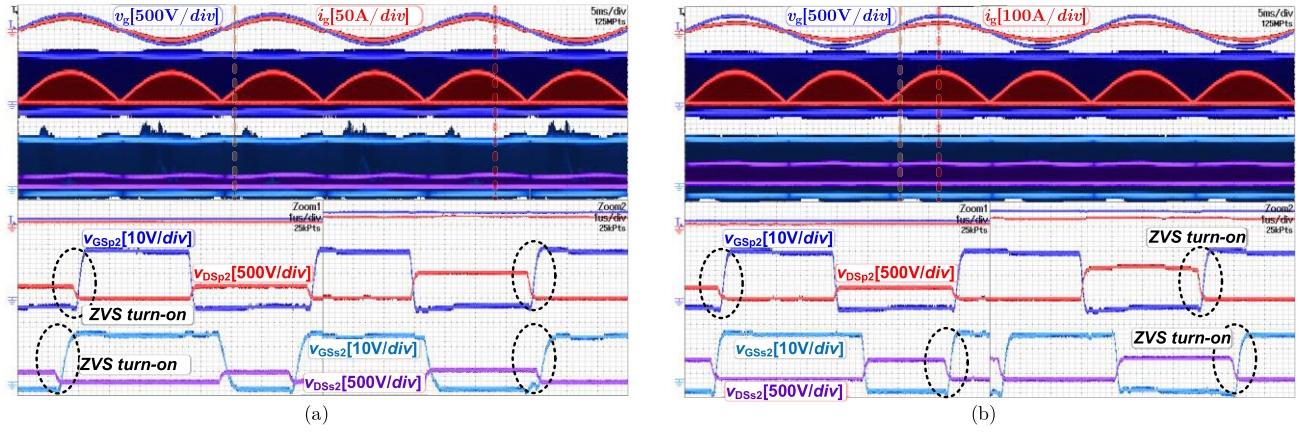

FIGURE 16. ZVS turn-on waveforms of the proposed converter under parallel configuration at input V_g of 230 V. (a) V_B = 150 V. (b) V_B = 480 V.

TABLE 3. The power is equally distributed among primary bridges, as shown in Fig.13.

Under 400 V class battery, v_{s1} and v_{s2} are set in parallel through L_s, as shown in Fig. 14(a) to efficiently charge 400V class batteries. In this mode, δ is set to zero, and ds plays a role in optimizing ZVS turn-on. Fig. 14(b) shows series configuration of v_{s1} and v_{s2} under 800 V EV charging system. In this mode, δ can be introduced according to conditions in (1). The ZVS turn-on output V_B range of the proposed converter is twice as conventional single-stage ZVS turn-on range [12], [13] due to proposed adjustable M_{vs}. At high V_B or high M_{vs}, ZVS turn-on of the primary switch (S_p) is more challenging, and vice versa. However, achieving ZVS turn-on for the secondary

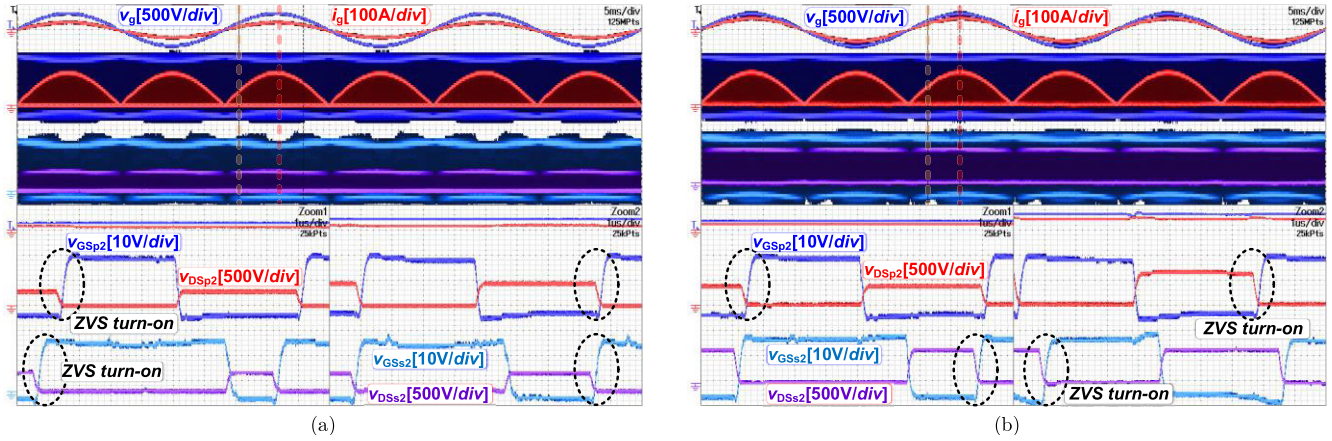

FIGURE 17. ZVS turn-on waveforms of the proposed converter under a series configuration (V_g = 230 V). (a) V_B = 350 V. (b) V_B = 860 V.

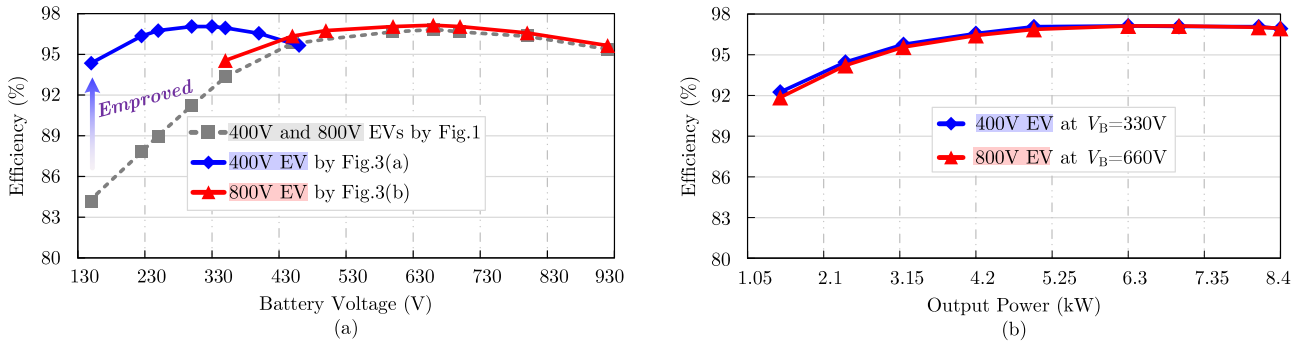

FIGURE 18. Performances of proposed converter under 400 V EV and 800 V class EV battery charging. (a) Conventional [12] and proposed converter according to charging line. (b). Proposed converter according to load.

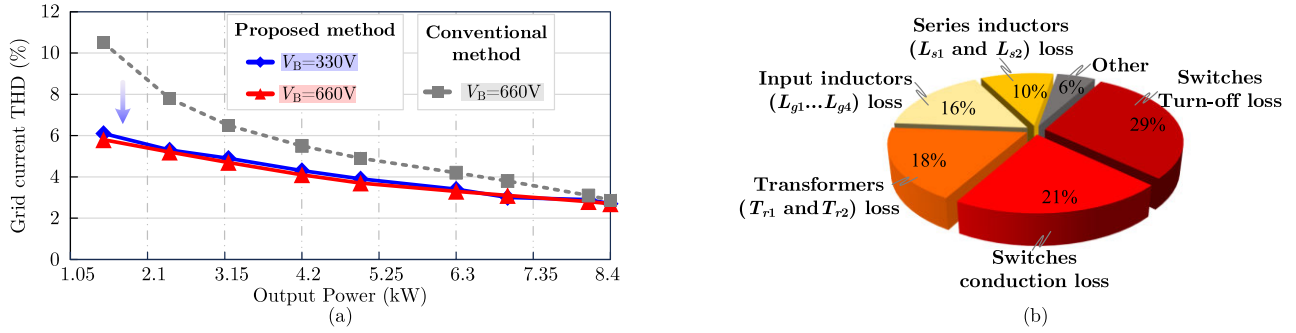

FIGURE 19. THD and loss distributions. (a) Grid current THD with proposed and conventional control method [12], [29]. (b) Loss breakdown of proposed charger at peak efficiency (P_o = 7 kW, V_B = 660 V).

switch (S_s) is difficult at low V_B (low M_{vs}), and vice versa.

In this work, M_{vs} is regulated to near unity to achieve ZVS for all switches. Fig. 16(a) and 16(b) shows ZVS turn-on of primary and secondary switches with proposed converter at different V_B under a parallel configuration. Similarly, Fig. 17(a) and 17(b) shows ZVS turn-on of primary and secondary switches of proposed converter under a series configuration.

Fig. 18(a) shows flat efficiency achieved by the proposed converter under 400 V and 800 V EV battery charging according to charging lines discussed above. Conventional converter achieved a significant drop in efficiency at low V_B due to HS turn-on and the large circulating current shown in Fig. 10.

Fig. 18(b) shows efficiency graphs of the proposed converter under parallel and series configuration according to load. Similar efficiency is achieved during 400 V and 800 V class battery charging due to optimal configurations of the proposed converter parameters such as L_s and v_s. Besides, with proposed instantaneous AC input current control, THD of less than 6% is achieved, including at light load, as shown

TABLE 4. Comparison of the proposed single-stage fast charger topology with other fast chargers.

Reference		**Proposed topology**	[12], [29]	[9]	[1], [7]	[7], [26]
Topology		Single-stage converter	Single-stage converter	Two-stage converter	Commercialized two-stage fast chargers	
Controller		Phase shift control (DPS, TPS)	Phase shift control (DPS) [27]	f_{sw} and Phase shift control (DPS, TPS)	Porsche Charge Box	ABB Tera CC HVC
E-capacitor (*Shorter lifespan*)		No	No	Yes	Yes	Yes
Relays		AC relays (*cheap*)	No	No	DC relays (*expensive*)	DC relays (*expensive*)
ZVS turn-on range		Wider range	Wide	Wide	Wide range	Wide range
Evaluated specifications	Output V_B	150 - 920 V DC	360 – 800 V DC	100 - 500 V DC	150-920 V DC	150-920 VDC
	Input V_g	230 V AC, 1-ϕ	230 V AC, 1-ϕ	240 – 400 V AC, 3-ϕ	480 VAC, 3-ϕ	480 V AC
	Power	8.4kW	3.6 kW	2.5 kW per module	360 kW	180 kW
	η_{peak}	**97.15%**	96.8%	95.1%	95%	95%

in Fig. 19(a). Furthermore, the loss of breakdown of the proposed converter given in Fig. 19(b).

VI. CONCLUSION

This article presented a reconfigurable, high-power, wide output voltage, high-efficiency, single-stage converter for fast charger applications. It achieved full ZVS turn-on for all switches and reduced circulating current with minimal optimization effort over a wide output voltage range. As a result, higher efficiency is achieved under both 400 V and 800 V EV compared to original single-stage converters [12], [13], [16]. High conversion efficiency of proposed converter is facilitated by relay matrices installed on the secondary side with minimum optimization effort. These relays are preset in advance before charging starts to avoid potential dynamic issues. Relay costs can be recouped quickly due to the high efficiency operation of the proposed battery fast charging converter.

An 8.4 kW per module laboratory prototype of fast charger is evaluated to validate the proposed concept. A peak efficiency of 97.15% is achieved at nominal points of both 400 V and 800 V EV battery classes. In addition, the proposed converter demonstrated flat efficiency according to the charging line, and low THD is achieved with proposed control methods including at light load. These make the proposed control an excellent choice for fast battery charging. Furthermore, the integration of input inductors and transformers may further improve the efficiency and power density of the charger.

ACKNOWLEDGMENT

The authors thank Infineon for supporting the sample switch devices (AIMCQ120R030M1T).

REFERENCES

[1] IEA, Paris, France. (2022). *Global EV Outlook 2022*. [Online]. Available: https://www.iea.org/reports/global-ev-outlook-2022

[2] A. Ahmad, Z. Qin, T. Wijekoon, and P. Bauer, "An overview on medium voltage grid integration of ultra-fast charging stations: Current status and future trends," *IEEE Open J. Ind. Electron. Soc.*, vol. 3, pp. 420–447, 2022, doi: 10.1109/OJIES.2022.3179743.

[3] S. Chaurasiya and B. Singh, "A bidirectional fast EV charger for wide voltage range using three-level DAB based on current and voltage stress optimization," *IEEE Trans. Transport. Electrific.*, vol. 9, no. 1, pp. 1330–1340, Mar. 2023, doi: 10.1109/TTE.2022.3201979.

[4] V. Monteiro, J. C. Ferreira, A. A. N. Meléndez, C. Couto, and J. L. Afonso, "Experimental validation of a novel architecture based on a dual-stage converter for off-board fast battery chargers of electric vehicles," *IEEE Trans. Veh. Technol.*, vol. 67, no. 2, pp. 1000–1011, Feb. 2018, doi: 10.1109/TVT.2017.2755545.

[5] M. A. Alharbi, A. M. Alcaide, M. Dahidah, P. Montero-Robina, S. Ethni, V. Pickert, and J. I. Leon, "Rotating phase shedding for interleaved DC–DC converter-based EVs fast DC chargers," *IEEE Trans. Power Electron.*, vol. 38, no. 2, pp. 1901–1909, Feb. 2023, doi: 10.1109/TPEL.2022.3211864.

[6] M. Safayatullah, M. T. Elrais, S. Ghosh, R. Rezaii, and I. Batarseh, "A comprehensive review of power converter topologies and control methods for electric vehicle fast charging applications," *IEEE Access*, vol. 10, pp. 40753–40793, 2022, doi: 10.1109/ACCESS.2022.3166935.

[7] H. Tu, H. Feng, S. Srdic, and S. Lukic, "Extreme fast charging of electric vehicles: A technology overview," *IEEE Trans. Transport. Electrific.*, vol. 5, no. 4, pp. 861–878, Dec. 2019, doi: 10.1109/TTE.2019.2958709.

[8] S. Rivera, S. M. Goetz, S. Kouro, P. W. Lehn, M. Pathmanathan, P. Bauer, and R. A. Mastromauro, "Charging infrastructure and grid integration for electromobility," *Proc. IEEE*, vol. 111, no. 4, pp. 371–396, Apr. 2023, doi: 10.1109/JPROC.2022.3216362.

[9] Y. Li, J. A. Anderson, M. Haider, J. Schäfer, J. Miniböck, J. Huber, G. Deboy, and J. W. Kolar, "Optimal synergetic operation and experimental evaluation of an ultracompact GaN-based three-phase 10-kW EV charger," *IEEE Trans. Transport. Electrific.*, vol. 10, no. 2, pp. 2377–2396, Jun. 2024, doi: 10.1109/TTE.2023.3297502.

[10] T. Friedli, M. Hartmann, and J. W. Kolar, "The essence of three-phase PFC rectifier systems—Part II," *IEEE Trans. Power Electron.*, vol. 29, no. 2, pp. 543–560, Feb. 2014, doi: 10.1109/TPEL.2013.2258472.

[11] S. Rivera, S. Kouro, S. Vazquez, S. M. Goetz, R. Lizana, and E. Romero-Cadaval, "Electric vehicle charging infrastructure: From grid to battery," *IEEE Ind. Electron. Mag.*, vol. 15, no. 2, pp. 37–51, Jun. 2021, doi: 10.1109/MIE.2020.3039039.

[12] H. Belkamel, H. Kim, and S. Choi, "Interleaved totem-pole ZVS converter operating in CCM for single-stage bidirectional AC–DC conversion with high-frequency isolation," *IEEE Trans. Power Electron.*, vol. 36, no. 3, pp. 3486–3495, Mar. 2021, doi: 10.1109/TPEL.2020.3016684.

[13] J. Lu, K. Bai, A. R. Taylor, G. Liu, A. Brown, P. M. Johnson, and M. McAmmond, "A modular-designed three-phase high-efficiency high-power-density EV battery charger using dual/triple-phase-shift control," *IEEE Trans. Power Electron.*, vol. 33, no. 9, pp. 8091–8100, Sep. 2018, doi: 10.1109/TPEL.2017.2769661.

[14] J. Everts, F. Krismer, J. Van den Keybus, J. Driesen, and J. W. Kolar, "Optimal ZVS modulation of single-phase single-stage bidirectional DAB AC–DC converters," *IEEE Trans. Power Electron.*, vol. 29, no. 8, pp. 3954–3970, Aug. 2014, doi: 10.1109/TPEL.2013.2292026.

[15] S. Kim, K. Kang, M. G. Geda, H.-P. Kieu, S. Choi, S. Lee, J. Yun, and J. Park, "A high-efficiency single-stage DAB microinverter with new switching modulation and integrated transformer," in *Proc. 11th Int. Conf. Power Electron. ECCE Asia (ICPE-ECCE Asia)*, Jeju Island, South Korea, May 2023, pp. 2498–2503, doi: 10.23919/ICPE2023-ECCEASIA54778.2023.10213715.
[16] D. Sha and S. Wang, "A single-stage natural power factor corrector based on dual active bridge DC–DC converter without inner current tracking loop," *IEEE Trans. Power Electron.*, vol. 36, no. 1, pp. 342–352, Jan. 2021, doi: 10.1109/TPEL.2020.3002241.
[17] F. Jauch and J. Biela, "Combined phase-shift and frequency modulation of a dual-active-bridge AC–DC converter with PFC," *IEEE Trans. Power Electron.*, vol. 31, no. 12, pp. 8387–8397, Dec. 2016, doi: 10.1109/TPEL.2016.2515850.
[18] H. Chung, S. Y. R. Hui, and K. K. Tse, "Reduction of power converter EMI emission using soft-switching technique," *IEEE Trans. Electromagn. Compat.*, vol. 40, no. 3, pp. 282–287, Aug. 1998, doi: 10.1109/15.709428.
[19] ABB Ltd. (Dec. 18, 2023). *ABB Terra HPC Fast Charging From 175 kW to 350 kW*. [Online]. Available: https://chargingshop.eu/product/abb-terra-hpc-fast-charging-station-output-from-175kw-to-350kw/
[20] S. Mukherjee, J. M. Ruiz, and P. Barbosa, "A high power density wide range DC–DC converter for universal electric vehicle charging," *IEEE Trans. Power Electron.*, vol. 38, no. 2, pp. 1998–2012, Feb. 2023, doi: 10.1109/TPEL.2022.3217092.
[21] ABB Ltd. (2020). *Electric Vehicle Infrastructure Terra HP High Power Charging UL*. Accessed: May 19, 2024. [Online]. Available: https://library.e.abb.com/public/49ff023197ba4be0a66ef56d733884ff/ABB_Terra-HP_UL_G2_Data-SheetR5.pdf?xsign=E6P88BtLcapu53LndUGz8u3PJXkqCnB+LPBmOacKTlWoCaaeJ9RJdC8ZS62pdFzp
[22] P. V. Harisyam and K. Basu, "A single-stage high-frequency-link medium voltage AC to DC converter for utility-scale grid integration of solar and storage," *IEEE Trans. Power Electron.*, early access, Aug. 6, 2024, doi: 10.1109/TPEL.2024.3439571.
[23] B. P. Do, M. G. Geda, J. Yun, K. Kang, S. Lee, and S. Choi, "Single-phase and three-phase compatible SingleStage OBC with 6-switches secondary side," in *Proc. IEEE 10th Int. Power Electron. Motion Control Conf. (IPEMC-ECCE Asia)*, Chengdu, China, May 2024, pp. 1908–1912, doi: 10.1109/IPEMC-ECCEASIA60879.2024.10567664.
[24] M. G. Geda, H. Song, P. D. Ba, B. Cho, S. Kim, and S. Choi, "Dual transformer-based single-stage converter for EV fast charger with flat efficiency characteristics," in *Proc. IEEE Appl. Power Electron. Conf. Expo. (APEC)*, Long Beach, CA, USA, Feb. 2024, pp. 1706–1711, doi: 10.1109/APEC48139.2024.10509315.
[25] A. Elezab, O. Zayed, A. Abuelnaga, and M. Narimani, "High efficiency LLC resonant converter with wide output range of 200–1000 V for DC-connected EVs ultra-fast charging stations," *IEEE Access*, vol. 11, pp. 33037–33048, 2023, doi: 10.1109/ACCESS.2023.3263486.
[26] ABB Ltd. (Dec. 18, 2023). *Terra DC Fast Chargers*. [Online]. Available: https://pulsal.ru/download/ABB/Terra/ABB_Brochure_Terra.pdf
[27] M. G. Geda, T.-T. Le, S. Kim, K. Kim, H.-P. Kieu, and S. Choi, "High efficiency and high-power quality modulation strategy for single-stage electrolytic capacitor-less on-board EV charger," in *Proc. 11th Int. Conf. Power Electron. ECCE Asia (ICPE-ECCE Asia)*, Jeju Island, South Korea, May 2023, pp. 1603–1608, doi: 10.23919/ICPE2023-ECCEASIA54778.2023.10213846.
[28] M. G. Geda, H. Song, B. P. Do, and S. Choi, "Light load efficiency enhancement strategy for single-stage AC–DC by using adaptive switching frequency," in *Proc. IEEE 10th Int. Power Electron. Motion Control Conf. (IPEMC-ECCE Asia)*, Chengdu, China, May 2024, pp. 2051–2055, doi: 10.1109/IPEMC-ECCEASIA60879.2024.10567907.
[29] R. Baranwal, G. F. Castelino, K. Iyer, K. Basu, and N. Mohan, "A dual-active-bridge-based single-phase AC to DC power electronic transformer with advanced features," *IEEE Trans. Power Electron.*, vol. 33, no. 1, pp. 313–331, Jan. 2018, doi: 10.1109/TPEL.2017.2669148.

MILLION GERADO GEDA (Member, IEEE) was born in Ethiopia, in 1991. He received the B.S. and M.S. degrees from Adama Science and Technology University (ASTU), Adama, Ethiopia, in 2016 and 2018, respectively. He is currently pursuing the Ph.D. degree with the Department of Electrical and Information Engineering, Seoul National University of Science and Technology (Seoul Tech), Seoul, South Korea.

In 2018, he joined the Department of Electrical Power and Control Engineering, ASTU, as a Lecturer. His research interests include high-efficiency power conversion technology for EV battery chargers and microgrids.

Mr. Geda was a recipient of the Best Prize Paper Award of IPEMC 2024-ECCE Asia.

SUNJU KIM (Student Member, IEEE) was born in South Korea, in 1994. He received the B.S. and M.S. degrees from the Department of Electrical and Information Engineering, Seoul National University of Science and Technology (Seoul Tech), Seoul, South Korea, in 2017 and 2019, respectively, where he is currently pursuing the Ph.D. degree.

His research interests include power conversion technologies for renewable energy systems and battery chargers for electric vehicles.

SEWAN CHOI (Fellow, IEEE) received the Ph.D. degree in electrical engineering from Texas A& M University, College Station, TX, USA, in 1995.

From 1985 to 1990, he was with Daewoo Heavy Industries, Incheon, South Korea, as a Research Engineer. From 1996 to 1997, he was a Principal Research Engineer with Samsung Electro-Mechanics Company, South Korea. In 1997, he joined the Department of Electrical and Information Engineering, Seoul National University of Science and Technology (Seoul Tech), Seoul, South Korea, where he is currently a Professor. He was the President of The Korean Institute of Power Electronics, Seoul, in 2021. His research interests include high power density power conversion technologies for electric vehicles and renewable energy systems.

Dr. Choi was a recipient of the Prize Paper Award of IEEE TRANSACTIONS ON POWER ELECTRONICS, in 2022. He served as the TPC Chair for ICPE2019-IEEE ECCE Asia held in Busan, South Korea, and the Chairperson of the IEEE PELS Seoul Section. He served as an Associate Editor for IEEE TRANSACTIONS ON POWER ELECTRONICS, from 2006 to 2022.